

Reverse Bias Behavior of Halide Perovskite Solar Cells

Andrea R. Bowring, Luca Bertoluzzi, Brian C. O'Regan, and Michael D. McGehee*

The future commercialization of halide perovskite solar cells relies on improving their stability. There are several studies focused on understanding degradation under operating conditions in light, but little is known about the stability of these solar cells under reverse bias conditions. Reverse bias stability is important because shaded cells in a module are put into reverse bias by the illuminated cells. In this paper, a phenomenological study is presented of the reverse bias behavior of halide perovskite solar cells and it is shown that reverse bias can lead to a partially recoverable loss in efficiency, primarily caused by a decrease in V_{OC} . A general mechanism is proposed, supported by drift–diffusion simulations, to explain how these cells breakdown via tunneling caused by accumulated ionic defects and suggests that the reversible loss in efficiency may be due to an electrochemical reaction of these defects. Finally, the implications of these phenomena are discussed and how they can possibly be addressed is also discussed.

1. Introduction

Halide perovskite solar cells have experienced an extraordinary rise in efficiency over the past few years, with record efficiencies for single junctions of 22.1%.^[1] Monolithic tandems involving perovskites also exhibit impressive efficiencies of 23.6% for perovskite-on-silicon^[2] and 19.0% for perovskite-on-perovskite.^[3] Halide perovskites are especially promising because they are solution processed at low temperatures, which could allow inexpensive manufacturing. One reason for the high performance of these devices despite their polycrystallinity is that the ionic defects that are likely to form have energies near the band edges.^[4]

Now that high efficiencies have been achieved, the next concern is whether these cells are stable under realistic operating conditions.^[5] There have been promising reports of stable performance over 1000 h at the maximum power point by changing composition and contacts.^[6,7] One important stability concern that has not been addressed yet is stability in reverse bias. In a solar cell module, a shaded cell ends up in reverse bias by being forced to pass the photocurrent of its unshaded neighbors. All

solar cells have a breakdown voltage (V_{BD}) at which current starts to flow in reverse bias. When current flows in reverse bias, the shaded cell dissipates power rather than producing it, and this can cause local heating, which damages the cell.^[8]

Silicon cells generally breakdown in reverse bias by avalanche breakdown; the carriers gain enough kinetic energy from the applied electric field to generate additional carriers through impact ionization. V_{BD} s for silicon cells are typically >15 V. If the pn junction is highly doped, the depletion width can narrow enough to allow tunneling in reverse bias. With either mechanism, breakdown current can get localized by uneven doping, crystalline defects, trace processing contaminants, etch sites, or edge effects causing damaging hot spots.

CIGS and CdTe exhibit V_{BD} s < 10 V and a decrease in V_{BD} under illumination. This has been attributed to tunneling through defects at the buffer layer/CIGS interface.^[9] Partial shading has been shown to cause local current flow and the damage is exacerbated by the light dependence of the V_{BD} , which causes even more of the current to selectively flow through the illuminated region. This can cause localized shunting those results primarily in a permanent decrease in fill factor.^[10]

Stability in reverse bias has not been explored for perovskite solar cells, but there have been studies of MAPbI₃ memristors,^[11–14] which require biasing in both forward and reverse directions, and photodetectors, which function in reverse bias.^[15] Some memristors operate via the formation of metallic filaments through the perovskite^[11,12] and others seem to function based on mobile defects in the perovskite.^[12,13] Photodiodes of the structure fluorine-doped tin oxide (FTO)/porous TiO₂/MAPbI₃/Spiro-OMeTAD/Au show current multiplication in reverse bias, which has been attributed to mobile ion accumulation.^[15] Mobile ions have also been used to explain hysteresis in current–voltage measurements.^[16,17] In most cells, preconditioning at lower voltages makes cells worse, which is why scans from J_{SC} to V_{OC} tend to give lower efficiencies. It has also been demonstrated that mobile ions can cause band bending that can turn a symmetric device with nonselective contacts into a diode that functions as a solar cell.^[18] Mobile ions likely also play an important role in the behavior of perovskite solar cells in reverse bias.

In this paper, we first present a phenomenological study of reverse bias breakdown in halide perovskite solar cells. We characterize cells that have been held at constant current in the dark as they would be in a series connected module if only one cell were completely shaded. We also provide constant voltage measurements. We show how the reverse breakdown

Dr. A. R. Bowring, Dr. L. Bertoluzzi, Prof. M. D. McGehee
Department of Materials Science and Engineering
Stanford University
Stanford, CA 94305, USA
E-mail: mmcgehee@stanford.edu

Dr. B. C. O'Regan
Sunlight Scientific
Berkeley, CA 94707, USA

 The ORCID identification number(s) for the author(s) of this article can be found under <https://doi.org/10.1002/aenm.201702365>.

process relates to mobile ions accumulating at the contacts and how prolonged reverse bias causes a partially reversible efficiency decay, which we attribute to a reaction of the mobile ionic species. Finally, we discuss the implications of the reverse bias behavior.

We focus on characterizing reverse bias breakdown in our most stable, efficient, and reproducible cell architecture: ITO/NiO/Cs_{0.17}FA_{0.83}Pb(I_{0.83}Br_{0.17})₃/C60/atomic layer deposited (ALD) SnO₂/ITO.^[7] The cesium and formamidinium were used to replace methylammonium to improve thermal stability and the ALD SnO₂ protects the cell during the sputtering of the top ITO. The top ITO electrode functions to hold volatile species in, keep moisture out, and do not react with the perovskite as readily as metal electrodes.

2. Reverse Bias Behavior

We tested Cs_{0.17}FA_{0.83}Pb(I_{0.83}Br_{0.17})₃ solar cells with a variety of organic and inorganic hole selective contacts as well as both metal and metal oxide electrodes. The breakdown voltages remain in the range from -1 to -4 V (Figure 1). We observe similar V_{BD} for cells made with MAPbI₃ and Cs_{0.15}FA_{0.85}Pb_{0.5}Sn_{0.5}I₃ (Figure S1a, Supporting Information), so this behavior is likely not unique to the perovskite we focus on here. It is also important to note that V_{BD} is subject to significant batch-to-batch variation (Figure S1b, Supporting Information). This batch-to-batch variation in V_{BD} is much larger than the variation in performance and could partially be due slightly different crystallinity or morphology which could be caused by different glovebox atmospheres or solution ages. Slight variations in stoichiometry could also change which mobile ionic species is dominant. This variation also likely has to do with factors that may change the interface energetics, such as humidity or slight variations in annealing or evaporation times.

Reverse bias of halide perovskite solar cells can cause a loss of efficiency by two different mechanisms. Some cells locally

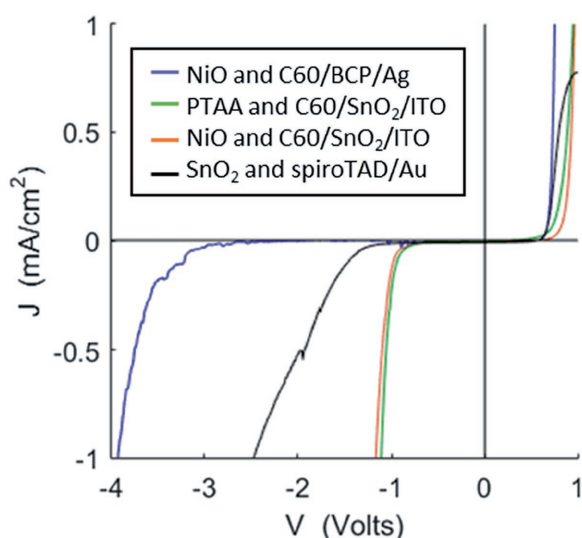


Figure 1. Dark J - V curves showing reverse bias breakdown for Cs_{0.17}FA_{0.83}Pb(I_{0.83}Br_{0.17})₃ cells with several different contacts.

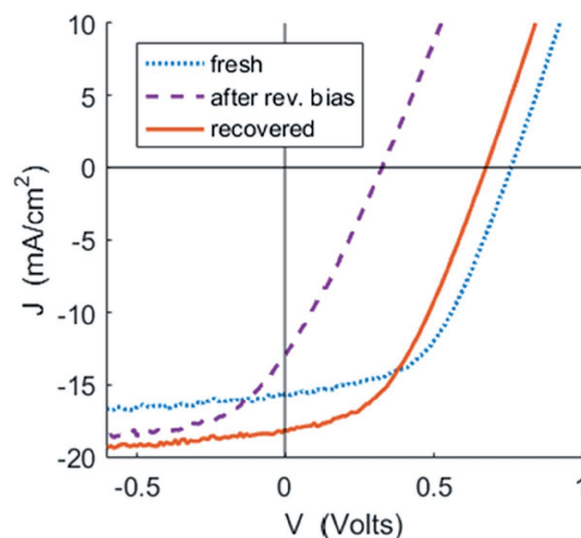


Figure 2. Light J - V curves of a cell when it was fresh, after 1 min at -20 mA cm^{-2} and after recovering over 3 h of maximum power point tracking.

shunt causing a decrease in fill factor as is seen in other technologies. However, some cells show nearly uniform reverse bias current across the entire cell that decreases efficiency without decreasing the shunt resistance. For these cells, we observed a small increase in series resistance and a substantial decrease in V_{OC} (Figure 2), which is more easily observed when the I - V curves are corrected for series resistance (Figure S3, Supporting Information). This cell was held at constant current in the dark which forced it into reverse bias. This is analogous to a single cell that is completely shaded in a series connected module. Interestingly, the efficiency drop is mostly recoverable after maximum power point tracking under one-sun illumination, which will be discussed further in the implications section.

To distinguish local shunting from uniform reverse bias current we used infrared (IR) thermal imaging. IR imaging measures the heating that occurs where the reverse bias current is flowing (Figure 3). Cells with ITO electrodes generally break down across the whole area (Figure 3a) whereas cells with silver or gold electrodes generally shunt locally, though some also undergo large area breakdown. We also find that some cells with ITO electrodes have local shunting due to extrinsic

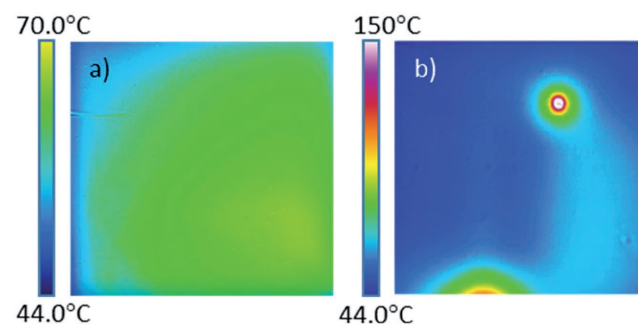


Figure 3. IR images of cells at -5 V showing a) uniform breakdown across the whole cell. The slight deviation from uniformity is due to the electrode pattern and the voltage drop across the fairly resistive top ITO electrode (Figure S2d, Supporting Information). b) Shunting due to local defects.

defects in the layers (Figure 3b). While it can be challenging to perform IR imaging of the reverse bias current with metal electrodes due to the reflectivity of the electrodes, other evidence suggests that local shunting frequently occurs. First, after reverse bias many cells act as resistors (Figure S2a, Supporting Information). Second, high reverse bias currents can locally melt the silver electrode (Figure S2b, Supporting Information). This local shunting may occur via silver filaments as has been observed in halide perovskite memristors.^[11,12] It is also possible to identify local shunting via the J - V curve. In this case the current almost instantaneously increases in reverse bias (Figure S2c, Supporting Information).

3. Mechanisms of the Reverse Bias Behavior

When localized shunts do not form, the reverse bias current likely occurs via tunneling rather than avalanche multiplication. The applied biases are too low to cause impact ionization and tunneling could be allowed by mobile ions accumulating at the contacts. **Figure 4** shows band diagrams for the case of mobile cations, such as iodide vacancies, calculated using the drift-diffusion model described in S4, Supporting Information. When contacts are initially applied, the built-in field causes positive vacancies to drift to the hole transport material (HTM) and accumulate in a very thin region at the absorber/HTM interface. A depletion region (similar to a Schottky barrier) forms at the interface with the electron transport material (ETM), as shown in Figure 4a. Therefore, at equilibrium at 0 V, the built-in potential is shielded in the bulk and concentrated at the contacts, mainly within the depletion region. Right after applying a reverse bias of -1 V (Figure 4b), the band bending induced by accumulated ions is not significant enough to allow tunneling. After the cell re-equilibrates by additional vacancies drifting toward the HTM, the band bending is more significant. When the reverse bias is large enough, holes can tunnel from the ETM to the valence band of the perovskite absorber producing current (Figure 4c). The asymmetry in the band diagram leads to the injection of one type of carrier at reverse bias.

We present a model with mobile vacancies because most recent experimental and theoretical studies present iodide vacancies as the main mobile species.^[19–21] The precise nature of the mobile species is not integral for our study because in our model the tunneling current is independent of the charge of the mobile ions. Previous studies identifying mobile species were on MAPbI_3 and do not necessarily reflect the $\text{Cs}_{0.17}\text{FA}_{0.83}\text{Pb}(\text{I}_{0.83}\text{Br}_{0.17})_3$ perovskite used in this work. For different perovskite compositions, the mobile species will probably vary. In fact, work by the Sargent group showed experimental evidence, supported by atomistic simulations, that the type of defect in methylammonium leads halides changes with slight variations in the stoichiometry.^[22] In our model, if the mobile species were anions, such as mobile halide interstitials, the band bending would be the same as the case for vacancies, but mirrored. The depletion region would be situated at the HTM/perovskite interface and the tunneling current would arise from electrons injected from the HTM to the absorber conduction band.

Using our drift-diffusion model, we have calculated that V_{BD} is inversely proportional to the concentration of mobile

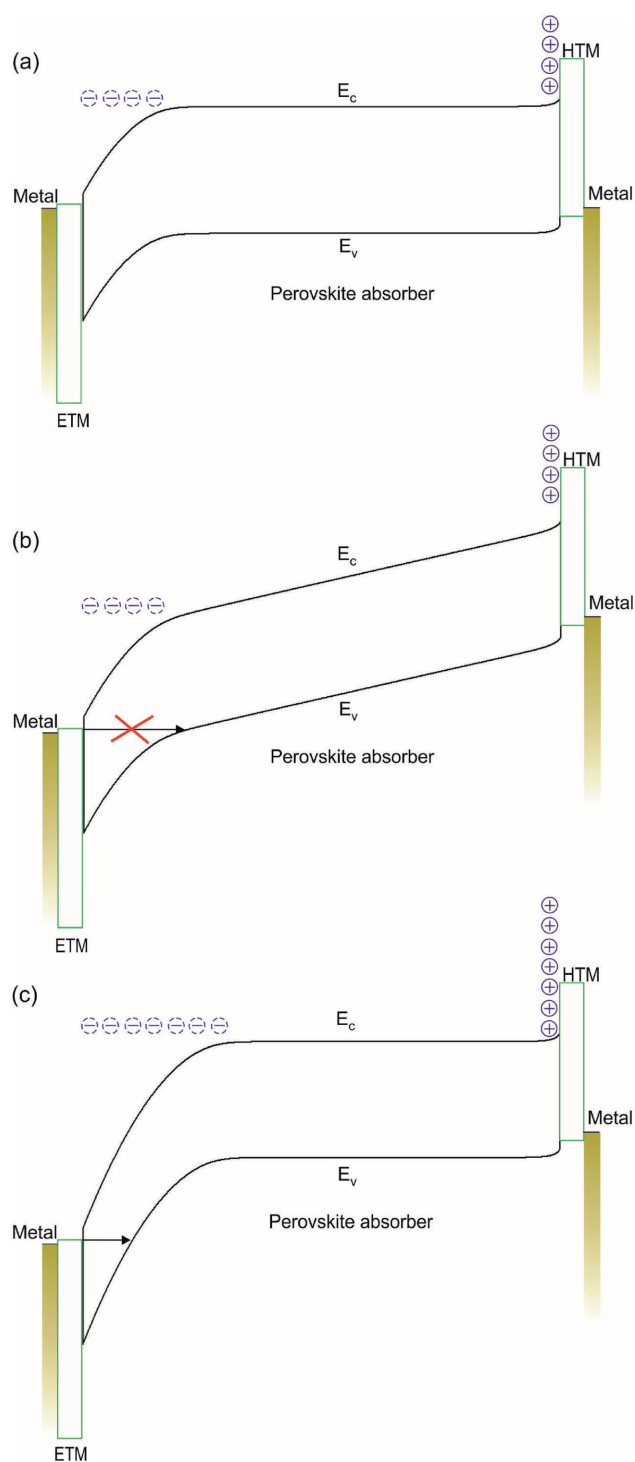


Figure 4. Band diagrams of the perovskite solar cell a) in dark equilibrium at 0 V b) right after applying a reverse bias (-1 V), and c) after ions have migrated to the contacts to equilibrate with the applied reverse bias. As ions accumulate at the contacts in reverse bias, the barrier to tunneling becomes narrower and allows holes to tunnel from the ETM to the perovskite absorber.

ions (Figure S5, Supporting Information). These calculations also show that for a tunneling process based only on mobile ion accumulation, the concentration of mobile ions necessary

for a V_{BD} of $-1V$ is around $5 \times 10^{19} \text{ cm}^{-3}$. This value is similar to the one reported in recent density functional theory (DFT) studies,^[23] but is significantly higher than other estimates of defect densities. The actual number of mobile ions is likely lower than our calculated value because there are a number of additional factors in an actual device that could lower the tunneling barrier. For example, the values for the work functions of the contacts were taken from literature and do not perfectly reflect the films we used. Additionally, our model is 1D and does not take into account that these films are polycrystalline and thus not perfectly uniform across the entire device area. There are reports showing that grain boundaries induce band bending and have higher ion mobilities and thus could have lower effective V_{BD} .^[24,25] Finally, the real material also likely has trap states within the tunneling barrier, which would lower the barrier via a trap-assisted tunneling process. These trap states could be introduced by the mobile ionic species themselves. Since we do not take into account these additional complexities, our model gives an upper bound for the ion concentration and complements the study by Calado et al.,^[26] who proposed a lower bound to the ion concentration of 10^{17} cm^{-3} . In addition, these simulations show that by engineering the interface and changing the number of ionic defects, one could alter the V_{BD} . This may be a desirable strategy to enhance reverse bias stability.

If the breakdown process were purely tunneling, we would expect the magnitude of the current at constant reverse bias voltage to increase after applying the reverse voltage as ions accumulate at the contacts and then remain constant once the ions built up (Figure S6, Supporting Information). Instead, the magnitude of the reverse bias current increases over the first 100 ms and then decays to a nonzero value (Figure 5). We attribute the fast initial increase to the ions drifting to the contacts to allow tunneling. Temperature dependent measurements support this hypothesis since at lower temperatures the initial increase in current slows down significantly (Figure S7a, Supporting Information). When we estimate the ionic mobility from the temperature dependent data using the transit time

(current peak) and Equation (1), we obtain $10^{-8} \text{ cm}^2 \text{ V}^{-1} \text{ s}^{-1}$ and an activation energy of 0.53 eV.

$$\mu = d^2 / Vt \quad (1)$$

where μ is mobility, d is the thickness of the film, and t is the transit time. Values for mobility reported in the literature are for methylammonium lead iodide measured via top contacts and vary from 1.5×10^{-9} ^[27] to 7.6×10^{-7} .^[28] Our calculated values of ionic mobility and activation energy are roughly consistent with reported values,^[29,30] so the initial increase in current could be explained by ions moving to the contact. Additionally, temperature dependent measurements also support the hypothesis of ionic motion. At low temperatures V_{BD} increases for a given scan rate because ions cannot move as quickly to allow tunneling (Figure S7b, Supporting Information).

Since halide perovskites are ionic conductors it is important to differentiate between electronic and ionic current. The integrated charge concentration from the current decay of Figure 5 is $\approx 4 \times 10^{22} \text{ cm}^{-3}$, which is higher than the total concentration of iodide atoms in the entire film. Thus the current must be electronic and not ionic. Therefore, the slow current decay indicates the presence of a process that slowly increases the barrier to tunneling. The probability, $P(E)$, for a hole with energy E to tunnel from the ETM to the valence band of the absorber depends on the tunneling barrier width and height as shown in Equation (2)

$$P(E) = \exp\left(-2w(E)\sqrt{\frac{2m^*}{h^2}\Phi_b(E)}\right) \quad (2)$$

where m^* is the effective mass of the perovskite, h is the Planck constant, w is the width of the tunneling barrier, and Φ_b its height. The key variables that determine the tunneling barrier height and width are the work function of both contacts, the applied bias, and the number of ions accumulated at the contacts. For example, increasing the work function of the ETM would increase the tunneling barrier height and width, while decreasing the work function of the HTM would increase its width. We see similar behavior for cells without a NiO HTM, which suggests that this slow process is not dependent on the HTM (Figure S8a, Supporting Information). In addition to decreasing the tunneling current, the slow process increases the V_{BD} and the series resistance in reverse bias (Figure S8b, Supporting Information). This slow process is likely occurring at a contact or interface given that it occurs after the ions have traversed the film.

In order to further understand the mechanism of this slow process we measured the electric field caused by accumulated ions using the method developed by Belisle et al.^[31] In reverse bias, ions accumulate and compensate the applied field and thus set up an electric field opposite to the applied field (Figure S10, Supporting Information). We measured the recovery of the ion-induced electric field (i.e., how fast ions moved back to their equilibrium position) after returning to 0 V. The ionic field recovers in one second (Figure S10e, Supporting Information), while it takes several minutes to hours for the slow degradation process to recover in the dark. This shows that the slow

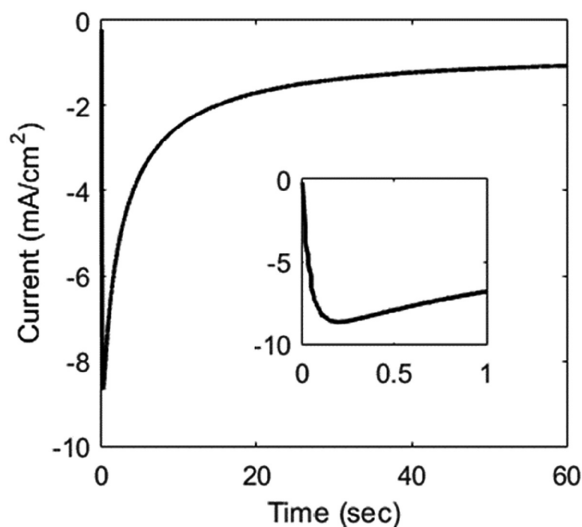


Figure 5. Reverse bias measurements of cells at a constant voltage of $-2V$. Inset shows first second.

process requires another mechanism in addition to the simple migration of ions. One possible explanation is that some of the involved mobile ions have been charge compensated, possibly by being oxidized or reduced. These charge compensated ions would no longer produce an electric field.

Evidence that an electrochemical reaction may be involved in the slow process shown in Figure 5 comes from its dependence on the amount of current that has flowed. Prebiasing at biases at which very little current flows has minimal effect on V_{BD} (Figure S9, Supporting Information). Additionally, the longer the device is held at reverse bias, the more pronounced the V_{oc} losses are. Finally, the process recovers faster in the light even at J_{SC} where the internal field should be similar to that in the dark (Figure S11, Supporting Information).

From our measurements, we can conclude that the process which leads to the current decay of Figure 5 and the V_{oc} losses of Figure 2 is dependent on the quantity of electronic and/or ionic charge that has flowed through the device. These observations support the hypothesis of an electrochemical oxidation/reduction reaction. Other possible processes that could be taking place at reverse bias are the formation of an insulating layer at one contact as ions move away or the formation of a dipole at the interface(s). These other processes by themselves are not sufficient to explain all our data. A more detailed study on this slow process is beyond the scope of this first study, but is underway.

4. Implications

It will be important to address the reverse bias degradation process described above for halide perovskites to become a viable commercial technology. Unfortunately, this process is not perfectly reversible and takes longer and longer to recover after each shading event (Figure 6). To simulate conditions of a series connected module where only a single cell is fully shaded we held a cell at the maximum power point current and cycled the light off (30 s) and on. After every cycle, the recovery time increases

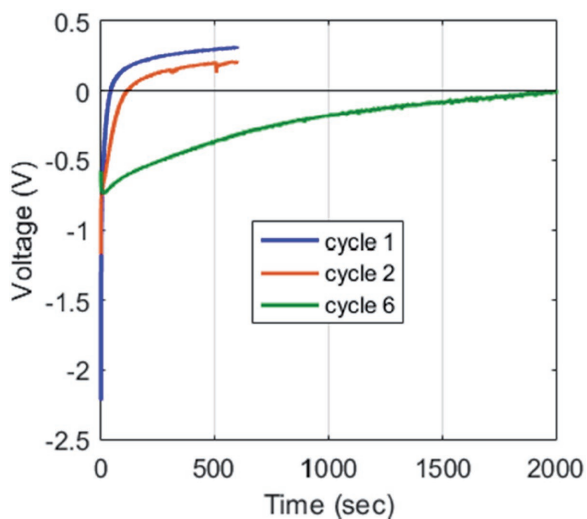


Figure 6. Cycling a cell that is being held at the maximum power point current in the dark (20 s) and light (600 s).

significantly. The second cycle takes twice as long to reach a positive voltage and the sixth cycle takes almost 50 times as long. This may be related to the performance fatigue that has been reported when cycling a cell between simulated day-night cycles, dark at 0 V and light at the maximum power point (MPP).^[32]

This degradation after multiple shading events could be addressed in multiple ways. First, using a thin film module design with long thin cells that are oriented perpendicular to the ground will decrease the probability that a significant fraction of a single cell will be shaded at once due to dirt or stationary objects (Figure S12, Supporting Information). If a module had long thin cells parallel to the ground, dirt or snow could accumulate on the bottom cell covering it and the shadow of a nearby tree or building would gradually move across the cells one by one as the day progressed. If module design does not adequately reduce the shading damage risk, reverse bias degradation could be addressed at the cell level by stopping the slow decay process, which is likely an electrochemical reaction of the ionic species at the perovskite/contact interface. It is unclear what this reaction is or precisely where it occurs, but if it occurs within the contact, putting an ion blocking layer between the perovskite and the contact could mitigate it. If the reaction were prevented, the reverse bias current would increase and then remain constant (Figure S6, Supporting Information) and each solar cell could effectively act as its own bypass diode and avoid damage. If this could be achieved, we would also want to lower V_{BD} to decrease the power dissipated in reverse bias and thus the damaging local heating.

Another option to prevent degradation after shading is to use bypass diodes in the module. However, bypass diodes would increase module costs, so in this case a larger V_{BD} would be required to minimize the number of diodes. For example, most silicon modules require approximately one bypass diode for every seventeen cells. V_{BD} in perovskites could be increased by decreasing the number of mobile ionic defects (Figure S5, Supporting Information). This could be achieved by increasing the crystallinity of the film or tuning the stoichiometry of the perovskite. Once V_{BD} is increased, bypass diodes are a good solution for single junction cells. However, additional challenges will limit their use in 4-terminal tandems. If the perovskite top cell with two higher-resistance semitransparent electrodes is designed like a traditional thin film module with long thin cells, a significant voltage drop would build up across the length of the cell because current will need to traverse the length to reach a bypass diode (Figure S13, Supporting Information). In the limit where the current through the cell is uniform the voltage drop in the electrode is expressed by Equation (3)

$$\Delta V = \frac{1}{2} R_{sh} J_{ph} L^2 \quad (3)$$

where R_{sh} is the sheet resistance of the electrode, J_{ph} is the photocurrent density produced by the neighboring unshaded cells and L is the length of the cell. Assuming both electrodes are ITO with a sheet resistance of 10 ohms per square, a length of 50 cm and a photocurrent of 20 mA cm⁻², there could be up to a 250 V drop. An additional solution would be needed to allow bypass diodes to work such as fine metal gridlines to decrease sheet resistance or different cell form factor.

5. Conclusion

In halide perovskite solar cells, current flows in reverse bias most likely due to tunneling mediated by mobile ions. The tunneling current decreases over time at constant voltage via a slower process. This process is likely an electrochemical reaction of the ions accumulating in or at the contact. As a result, both the series resistance and V_{BD} increase and V_{OC} decreases. This decrease in efficiency is mostly recoverable. Therefore, infrequent random shading, such as from clouds, will likely not be an issue. However, there may be a problem with daily shading caused by a tree or other nearby stationary objects, which would be more of an issue in residential applications. One solution is to design cells that breakdown at lower voltages to decrease power dissipation. The other would be to design cells with larger V_{BD} and introduce bypass diodes. In this study, we focused on the mechanism of breakdown in full dark conditions. Future studies will need to be done on partial shading, which can stress cells even more because the current selectively flows through the illuminated region creating localized heating at the edge of the shaded region.^[33] Finally, V_{BD} will be a useful metric for researchers to measure and report as they develop new architectures and chemistries to assist the perovskite community in moving toward the most commercially promising device.

6. Experimental Section

The solar cells were of the structure ITO/NiO/Cs_{0.17}FA_{0.83}Pb(I_{0.83}Br_{0.17})₃/C60/SnO₂/ITO were fabricated in a method documented elsewhere.^[7] Current density–voltage (J – V) measurements on solar cell devices were performed with a Keithley 2400 Series source meter, under 100 mW cm⁻² AM 1.5 irradiance (Abet Class AAB sun 2000 simulator). The light source was calibrated with an NREL-calibrated KG5 filtered Si reference cell. During testing, the solar cells were masked to 0.38 cm², whereas the area of the sputtered to ITO electrode was ≈1 cm². Temperature dependent reverse bias current transients were measured in an evacuated, liquid nitrogen cooled Janus ST-100 cryostat also using a Keithley 2400 source meter.

Photocurrent transient measurements were measured using the setup introduced in Belisle et al.^[31] The IR temperature images were measured using a high resolution infrared microscope with a 1X objective (QFI/Infrascopes). Scanning electron micrographs were taken using a FEI XL30 Sirion scanning electron microscope (SEM) with FEG source operated at an accelerating voltage of 5 kV. Drift–diffusion modeling is described in the supplement (Figure S4, Supporting Information).

Supporting Information

Supporting Information is available from the Wiley Online Library or from the author.

Acknowledgements

The authors thank the Bay Area Photovoltaic Consortium and the Swiss National Science Foundation (project P2SKP2_168301) for financial support. The authors are very grateful to Kevin Bush and Mico Diaz for assistance in cell fabrication, Axel Palmstrom for assistance in depositing the ALD SnO₂ layer, Sunpreme for sputtering top ITO contacts, Mark Goodson, Ian McKay, and Rahul Kini for assistance with IR imaging and Sarah Kurtz and Tim Silverman for helpful discussions.

Conflict of Interest

The authors declare no conflict of interest.

Keywords

drift–diffusion modeling, halide perovskites, ionic conduction, photovoltaics, reverse bias, stability

Received: August 28, 2017

Revised: September 24, 2017

Published online: December 4, 2017

- [1] W. S. Yang, B.-W. Park, E. H. Jung, N. J. Jeon, Y. C. Kim, D. U. Lee, S. S. Shin, J. Seo, E. K. Kim, J. H. Noh, S. Il Seok, *Science* **2017**, 356, 1376.
- [2] T. Duong, Y. Wu, H. Shen, J. Peng, X. Fu, D. Jacobs, E.-C. Wang, T. C. Kho, K. C. Fong, M. Stocks, E. Franklin, A. Blakers, N. Zin, K. McIntosh, W. Li, Y.-B. Cheng, T. P. White, K. Weber, K. Catchpole, *Adv. Energy Mater.* **2017**, 7, 1700228.
- [3] A. Rajagopal, Z. Yang, S. B. Jo, I. L. Braly, P.-W. Liang, H. W. Hillhouse, A. K.-Y. Jen, *Adv. Mater.* **2017**, 29, 1702140.
- [4] W.-J. Yin, T. Shi, Y. Yan, *Appl. Phys. Lett.* **2014**, 104, 63903.
- [5] T. Leijtens, G. E. Eperon, N. K. Noel, S. N. Habisreutinger, A. Petrozza, H. J. Snaith, *Adv. Energy Mater.* **2015**, 5, 1.
- [6] A. Mei, X. Li, L. Liu, Z. Ku, T. Liu, Y. Rong, M. Xu, M. Hu, J. Chen, Y. Yang, M. Grätzel, H. Han, *Science* **2014**, 345, 295.
- [7] K. A. Bush, A. F. Palmstrom, Z. J. Yu, M. Boccard, R. Cheacharoen, J. P. Mailoa, D. P. McMeekin, R. L. Z. Hoye, C. D. Bailie, T. Leijtens, I. M. Peters, M. C. Minichetti, N. Rolston, R. Prasanna, S. Sofia, D. Harwood, W. Ma, F. Moghadam, H. J. Snaith, T. Buonassisi, Z. C. Holman, S. F. Bent, M. D. McGehee, *Nat. Energy* **2017**, 2, 17009.
- [8] T. J. Silverman, M. G. Deceglie, X. Sun, R. L. Garris, M. A. Alam, C. Deline, S. Kurtz, *IEEE J. Photovolt.* **2015**, 5, 1742.
- [9] P. Szaniawski, J. Lindahl, T. Törndahl, U. Zimmermann, M. Edoff, *Thin Solid Films* **2013**, 535, 326.
- [10] T. J. Silverman, L. Mansfield, I. Repins, S. Kurtz, *IEEE J. Photovolt.* **2016**, 6, 1333.
- [11] K. Yan, M. Peng, X. Yu, X. Cai, S. Chen, H. Hu, B. Chen, X. Gao, B. Dong, D. Zou, *J. Mater. Chem. C* **2016**, 4, 1375.
- [12] E. Yoo, M. Lyu, J.-H. Yun, C. Kang, Y. Choi, L. Wang, *J. Mater. Chem. C* **2016**, 4, 7824.
- [13] C. Gu, J.-S. Lee, *ACS Nano* **2016**, 10, 5413.
- [14] E. J. Yoo, M. Lyu, J. Yun, C. J. Kang, Y. J. Choi, L. Wang, *Adv. Mater.* **2015**, 27, 6170.
- [15] K. Domanski, W. Tress, T. Moehl, M. Saliba, M. K. Nazeeruddin, M. Grätzel, *Adv. Funct. Mater.* **2015**, 25, 6936.
- [16] E. L. Unger, E. T. Hoke, C. D. Bailie, W. H. Nguyen, A. R. Bowring, T. Heumüller, M. G. Christoforo, M. D. McGehee, *Energy Environ. Sci.* **2014**, 7, 3690.
- [17] H. Yu, H. Lu, F. Xie, S. Zhou, N. Zhao, *Adv. Funct. Mater.* **2016**, 26, 1411.
- [18] Y. Yuan, J. Chae, Y. Shao, Q. Wang, Z. Xiao, A. Centrone, J. Huang, *Adv. Energy Mater.* **2015**, 5, 1500615.
- [19] A. Senocrate, I. Moudrakovski, G. Y. Kim, T.-Y. Yang, G. Gregori, M. Grätzel, J. Maier, *Angew. Chem., Int. Ed.* **2017**, 1.
- [20] E. Mosconi, F. De Angelis, *ACS Energy Lett.* **2016**, 1, 182.
- [21] H. Lee, S. Gaiaschi, P. Chapon, A. Marronnier, H. Lee, J.-C. Vanel, D. Tondelier, J.-E. Bourée, Y. Bonnassieux, B. Geffroy, *ACS Energy Lett.* **2017**, 2, 943.

- [22] A. Buin, R. Comin, J. Xu, A. H. Ip, E. H. Sargent, *Chem. Mater.* **2015**, *27*, 4405.
- [23] A. Walsh, D. O. Scanlon, S. Chen, X. G. Gong, S.-H. Wei, *Angew. Chem., Int. Ed.* **2015**, *54*, 1791.
- [24] Y. Yuan, J. Huang, *Acc. Chem. Res.* **2016**, *49*, 286.
- [25] J. Li, J.-Y. Ma, Q.-Q. Ge, J. Hu, D. Wang, L.-J. Wan, *ACS Appl. Mater. Interfaces* **2015**, *7*, 28518.
- [26] P. Calado, A. M. Telford, D. Bryant, X. Li, J. Nelson, B. C. O'Regan, P. R. F. Barnes, *Nat. Commun.* **2016**, *7*, 13831.
- [27] Y. Yuan, J. Chae, Y. Shao, Q. Wang, Z. Xiao, A. Centrone, J. Huang, *Adv. Energy Mater.* **2015**, *5*, 1.
- [28] M. N. F. Hoque, N. Islam, Z. Li, G. Ren, K. Zhu, Z. Fan, *ChemSusChem* **2016**, *9*, 2692.
- [29] W. Tress, *J. Phys. Chem. Lett.* **2017**, *8*, 3106.
- [30] N. Vicente, G. Garcia-Belmonte, *Adv. Energy Mater.* **2017**, *7*, 1700710.
- [31] R. A. Belisle, W. H. Nguyen, A. R. Bowring, P. Calado, X. Li, S. J. C. Irvine, M. D. McGehee, P. R. F. Barnes, B. C. O'Regan, *Energy Environ. Sci.* **2017**, *10*, 192.
- [32] F. Huang, L. Jiang, A. R. Pascoe, Y. Yan, U. Bach, L. Spiccia, Y. B. Cheng, *Nano Energy* **2016**, *27*, 509.
- [33] S. Dongaonkar, S. Member, C. Deline, M. A. Alam, *IEEE J. Photovolt.* **2013**, *3*, 1367.